Available online at www.sciencedirect.com
SCIENCE DIRECT
Catalysis Today 107–108 (2005) 578–588
CATALYSIS TODAY
www.elsevier.com/locate/cattod

NiMo catalysts supported on titania-modified SBA-16 for 4,6-dimethyldibenzothiophene hydrodesulfurization

Juan Carlos Amezcua [a], Lilia Lizama [a], Cecilia Salcedo [a], Ivan Puente [a], Jose Manuel Domínguez [b], Tatiana Klimova [a,*]

[a] *Departamento de Ingeniería Química, Facultad de Química, UNAM, Cd. Universitaria, C.P. 04510 México D.F., México*
[b] *Programa de Ingeniería Molecular, Instituto Mexicano del Petróleo, Eje Central Lázaro Cárdenas #152, C.P. 07730 México D.F., México*

Available online 15 August 2005

Abstract

A series of Ti-containing mesoporous SBA-16 supports and the respective NiMo catalysts were prepared to study the effect of the method for support preparation and TiO_2 loading on the dispersion of titania, characteristics of Ni and Mo surface species and their catalytic activities in the 4,6-dimethyldibenzothiophene hydrodesulfurization (HDS). The solids prepared were characterized by N_2 physisorption, X-ray diffraction (XRD), UV–vis diffuse reflectance spectroscopy (DRS), FT–Raman spectroscopy, temperature-programmed reduction (TPR), chemical analysis and HRTEM. Titania was incorporated to purely siliceous SBA-16 support by two post-synthetic methods: chemical grafting and incipient wetness impregnation. The results show that Ti-SBA-16 supports with different TiO_2 content and dispersion can be obtained without substantial loss of SBA-16 characteristics. The best dispersion of TiO_2 in the SBA-16 pore channels was obtained by the grafting method (DRS, FT–Raman). However, titania loading in this case was limited to 15.1 wt.% TiO_2. Samples prepared by impregnation show the presence of different Ti species: isolated Ti species and small anatase clusters (inside the mesopore channels of SBA-16) and anatase crystallites (on the external surface), even for low titania loadings (XRD). Crystal size of anatase phase increased with titania loading. It was found that TiO_2 incorporation in the SBA-16 support leads to stronger interaction of Mo and Ni oxidic species with the support (TPR) providing better dispersion to the sulfided metal species (HRTEM). NiMo catalysts supported on Ti-modified SBA-16 showed high activity in 4,6-dimethyldibenzothiophene HDS. It can be concluded, therefore, that Ti-SBA-16 materials prepared by post-synthetic routes show promising features as supports for Mo-based hydrotreating catalysts.

Keywords: Ti-SBA-16; Mesoporous molecular sieves; NiMo catalysts; Hydrodesulfurization; 4,6-Dimethyldibenzothiophene

1. Introduction

Nowadays, much effort is made aimed at improvement of hydrodesulfurization (HDS) catalysts in view of the greater concern over environmental pollution by automobiles and consequently more stringent limitations to sulfur contents in gasoline and diesel fractions. Mo-based hydrotreating catalysts supported on γ-alumina have been traditionally used for hydrotreatment of oil feedstock (HDT) [1,2]. Recently, in order to obtain more active HDS catalysts, many approaches have been followed, among which variation of support is an important one. Different materials have been assayed as supports for HDS catalysts, namely SiO_2 [3,4], MgO [5], ZrO_2 [6], TiO_2 [3,7], carbon [8], microporous zeolites like NaY [9], USY [10], mesoporous materials like MCM-41 [11–14], SBA-15 [15], as well as their different combinations like mixed oxides [16], alumina-zeolite [17] or alumina-MCM-41 composites [18], etc. A detailed analysis of the support effect can be found in recent reviews [16,19].

Among different supports and their combinations, TiO_2 has attracted attention due to the higher intrinsic HDS activity demonstrated by Mo catalysts supported on this oxide [7,20]. The high activity has been attributed mostly to the formation of well-dispersed molybdena species that arise from the relatively high density of reactive hydroxyl groups on the

* Corresponding author. Tel.: +52 55 56225371; fax: +52 55 56225371.
E-mail address: klimova@servidor.unam.mx (T. Klimova).

0920-5861/$ – see front matter © 2005 Elsevier B.V. All rights reserved.
doi:10.1016/j.cattod.2005.07.018

TiO_2 surface. Additionally, it was found that titania enhances the reduction and sulfidation of Mo^{6+} oxide species making the formation of catalytically active MoS_2 easier. However, titania supports present one important disadvantage: they generally have low surface area and porosity [21]. Because of this problem, some attempts to obtain titania-based supports with high surface area have been made in recent years. For example, Chiyoda Corporation successfully developed a novel method for preparing mesoporous TiO_2 with a specific surface area of 120 m^2/g that provides the opportunity to prepare the catalyst with a good Mo dispersion up to 10–12 wt.% Mo loading [22]. Another possible route to achieve this goal is to cover a support with appropriate textural properties with TiO_2. Thus, promising results were obtained when titania was incorporated on the surface of mesoporous molecular sieve MCM-41 with pores of about 30 Å in diameter and surface areas of about 1200 m^2/g [23]. A substantially better dispersion of Mo was observed on MCM-41 supports modified with TiO_2 by post-synthetic methods. However, the parent MCM-41 type materials have poor stability, which represents a serious limitation to their practical applications [24,25].

Recently, a novel family of mesoporous silicas (SBA) was synthesised by using neutral organic triblock copolymers [26–28]. These new materials have larger pores, thicker pore walls and higher hydrothermal stability compared to MCM-41 [28–31]. Purely siliceous SBA-15 material has already been tested as support for WS_2 active phase. However, because of very weak metal-support interaction, ultrasonic deposition of WS_2 had been used to achieve a better dispersion of W sulfided species [15]. In our group, a series of Al-containing mesoporous molecular sieves SBA-16 and the respective NiMo catalysts were prepared and tested in 4,6-dimethyldibenzothiophene HDS [32]. It was found that aluminum incorporation in the SBA-16 support provides better dispersion to deposited Ni and Mo active species and increases their catalytic activity.

In the present work, with the aim of obtaining SBA-type supports that provide good Mo dispersion and therefore high HDS activity, we prepared and characterized a series of Ti-modified SBA-16 supports and the respective NiMo catalysts, which were evaluated in the 4,6-dimethyldibenzothiophene (4,6-DMDBT) HDS reaction. Purely siliceous SBA-16 ($Im\bar{3}m$) was selected as a parent material to be modified with titania, because of its attractive three-dimensional mesoporous structure, which consists of large spherical cavities arranged in a body-centered cubic array and connected through smaller mesoporous openings along the (1 1 1) directions [33]. The exact pore diameter of large cavities and mesoporous openings of SBA-16 material is still a matter of discussion, because different pore size values are obtained by the BET technique (54 Å diameter [27]) and from high-resolution electron microscopy (95 Å diameter for large cavities and 23 Å for mesoporous openings [33]). Nevertheless, SBA-16 has been considered to be suitable for catalyst supports because of super-large cage, high surface area, high thermal stability and, especially, three-dimensional channel connectivity, which provides more favorable mass transfer kinetics than the unidirectional pore system of other hexagonal mesoporous phases [30]. Titania was incorporated in this parent SBA-16 by two post-synthetic methods, viz., chemical grafting and incipient wetness impregnation [34,35]. These methods were chosen because Ti incorporation into SBA structure by direct synthesis appears unlikely since these materials are synthesised in strongly acidic media (2 M HCl). Additionally, post-synthetic methods have serious advantages in comparison with Ti incorporation during hydrothermal synthesis of SBA materials, namely (i) higher Ti loading without substantial loss of the parent SBA structure and texture, (ii) location of Ti species on the support surface that makes them accessible for the interaction with NiMo active species and (iii) possibility of fine tuning of the characteristics of the deposited TiO_2 species by modifying the preparation procedure used [23,35].

The aim of the present work is to study the effect of the preparation method of titania-covered SBA-16 supports and TiO_2 loading on the dispersion of titania, characteristics of the Ni and Mo supported species, and the performance of the obtained catalysts in the 4,6-dimethyldibenzothiophene hydrodesulfurization.

2. Experimental

2.1. Support and catalyst preparation

The pure siliceous cubic $Im\bar{3}m$ SBA-16 (Si-SBA-16 sample) was prepared according to the previously described procedure [32] using the triblock copolymer Pluronic F127 ($EO_{106}PO_{70}EO_{106}$, BASF) as the structure-directing agent and tetraethyl orthosilicate (TEOS) as the silica source. Pluronic F127 (4 g) was dissolved in water (30 ml) and 2 M HCl (120 ml) at 25 °C. Then TEOS (8.50 g) was added to the solution. The mixture was stirred at 25 °C for 20 h and then aged at 100 °C for 24 h without stirring. The solid product was recovered by filtration, washed with deionized water, and air-dried at room temperature. Calcination was carried out in static air at 550 °C for 6 h. This Si-SBA-16 was used as a parent material to produce Ti-containing SBA-16.

Ti-modified SBA-16 supports were prepared using two methods of post-synthetic Ti incorporation: chemical grafting (G) and incipient wetness impregnation (I) [23,34,35]. In both cases, titanium(IV) isopropoxide ($Ti(i\text{-}PrO)_4$, Aldrich, 97%) was used as titania source and dry ethanol as the solvent (EtOH, Aldrich, 99.999%). In the grafting procedure, calcined Si-SBA-16 was slurried in dry EtOH containing $Ti(i\text{-}PrO)_4$ for 1 h. To eliminate the excess $Ti(i\text{-}PrO)_4$, the filtered material was washed with dry EtOH three times. The solid was then dried in air at room temperature and calcined in static air at 550 °C for 5 h. For the preparation of the titanium-impregnated SBA-16 samples, calcined Si-SBA-16 was

impregnated with an ethanolic solution containing the required amount of Ti(i-PrO)$_4$. Then, the samples were dried and calcined as described above. In this case, no additional washing was performed after Ti incorporation. Hereafter, Ti-containing SBA-16 materials will be denoted as Ti-SBA-16(M-x) samples, where M represents the method used for Ti incorporation in the support (M = G for chemical grafting, or I for incipient wetness impregnation) and x is the real TiO_2 content (wt.%) in each sample.

NiMo/SBA-16 catalysts were prepared by a standard incipient wetness technique. The calcined supports were impregnated successively using aqueous solutions of ammonium heptamolybdate, $(NH_4)_6Mo_7O_{24}{\cdot}4H_2O$ (Aldrich), and nickel nitrate, $Ni(NO_3)_2{\cdot}6H_2O$ (Aldrich). Mo was impregnated first. After each impregnation, the catalysts were dried (100 °C, 24 h) and calcined (500 °C, 2 h). The nominal composition of the catalysts was 12 wt.% MoO_3 and 3 wt.% NiO. Hereafter, the catalysts will be denoted as NiMo/ corresponding support.

2.2. Support and catalyst characterization

The supports and catalysts were characterized by N_2 physisorption, X-ray diffraction (XRD), UV–vis diffuse reflectance spectroscopy (DRS), FT–Raman spectroscopy, temperature-programmed reduction (TPR), chemical analysis and HRTEM. N_2 adsorption–desorption isotherms were measured with a Micromeritics ASAP 2000 automatic analyzer at liquid N_2 temperature. Prior to the experiments, the samples were degassed ($P < 10^{-1}$ Pa) at 270 °C for 6 h. Specific surface areas were calculated by the BET method (S_{BET}), the pore volume (V_P) was determined by nitrogen adsorption at a relative pressure of 0.98. Pore size distributions were found from the adsorption isotherms by the BJH method taking into account that the ink-bottle shaped pores of SBA-16 type materials prevent the use of the desorption branch of the isotherm for the determination of the pore size. The microporous area was estimated using the correlation of t-Harkins & Jura (t-plot method). XRD patterns were recorded in the $3^\circ \leq 2\Theta \leq 90^\circ$ range on a Siemens D5000 diffractometer, using Cu Kα radiation (λ = 1.5406 Å) and a goniometer speed of 1° (2Θ) min^{-1}. Small-angle XRD (2Θ = 1–10°) was performed on a Bruker D8 Advance diffractometer using small divergence and scattering slits of 0.05°. UV–vis–NIR electronic spectra of the samples were recorded in the wavelength range 250–2500 nm using a Cary |5E| spectrophotometer equipped with a diffuse reflectance attachment. $BaSO_4$ was used as reference. The laser Raman spectra were recorded in the 400–4000 cm^{-1} range on a Nicolet 950 FT spectrometer. A Nd-YAG laser was used as the excitation source with a slit width setting of 4 cm^{-1}. Signal detection was achieved with an InGaAs detector. TPR experiments were carried out in an automated ISRI-RIG-100 characterization system equipped with a TC detector. In the TPR experiments, the samples were pretreated in situ at 500 °C for 2 h under air flow and cooled in an Ar stream. The reduction step was performed with an Ar/H_2 mixture, with a heating rate of 10 °C/min, up to 1000 °C. The chemical analysis of the supports and NiMo catalysts was made by Desert Analytics (USA). High resolution transmission electron microscopy (HRTEM) studies were performed using a Jeol 2010 microscope (resolving power 1.9 Å). The solids were ultrasonically dispersed in heptane and the suspension was collected on carbon coated grids. Slab length and layer stacking distributions of MoS_2 crystallites in each sample were established from the measurement of at least 300 crystallites detected on several HRTEM pictures taken from different parts of the same sample dispersed on the microscope grid.

2.3. Catalytic activities

The 4,6-DMDBT HDS activity tests were performed in a batch reactor at 300 °C and 7.3 MPa total pressure for 8 h. Prior to the catalytic activity tests, the catalysts were sulfided ex situ in a tubular reactor at 400 °C for 4 h in a stream of 15 vol.% of H_2S in H_2 under atmospheric pressure. The course of the reaction was followed by withdrawing aliquots each hour and analyzing them on an HP-6890 chromatograph. To corroborate product identification, the product mixture was analyzed on a Hewlett Packard GC–MS instrument.

3. Results and discussion

3.1. Supports

The real TiO_2 loading in the synthesised SBA-16 molecular sieves are given in Table 1. The results from chemical analysis show that Ti-SBA-16 support prepared by chemical grafting has 15.1 wt.% TiO_2. In the preparation of this sample a larger amount of titanium (20 wt.% TiO_2) was used. However, only 75% of the total titanium was retained on the SBA-16 surface as a result of the chemical interaction with the silanol groups of the support, whereas the Ti in excess was eliminated by washing with dry ethanol. On the basis of this result, the monolayer capacity of SBA-16 surface can be estimated as about 1.4 Ti atoms/nm^2. This value is far below the silanol surface density of ∼3.7 OH/nm^2 that has been previously reported for SBA-15 material [36]. From the above results, it can be inferred, therefore, that the monolayer-like distribution of titania takes place in this case, in which each titanium atom is retained on the surface by one or two Ti–O–Si linkages. In addition, the existence of some isolated hydroxyls inert to the interaction with titanium isopropoxide at room temperature can also be expected on the surface of the parent SBA-16 material, as it has been previously observed for different silica supports [37]. For all the Ti-SBA-16(I-x) samples prepared by incipient wetness impregnation, real TiO_2 contents are in close agreement with the expected TiO_2 loadings, which were 10.0, 20.0 and 30.0 wt.% TiO_2 (Table 1). This means that the titanium has been mostly incorporated into the siliceous SBA-16 by this technique.

Table 1
Textural characteristics and chemical compositions of SBA-16 molecular sieves

Sample	Method of Ti incorporation[a]	TiO_2 wt.%[b]	S_{BET} (m^2/g)	S_μ[c] (m^2/g)	V_P (cm^3/g)	V_μ[c] (cm^3/g)	D_P[d] (Å)	NS_{BET}[e]
Si-SBA-16	–	–	920	107	0.602	0.047	52	1.0
Ti-SBA-16(G-15)	CG	15.1	818	112	0.568	0.048	50	1.0
Ti-SBA-16(I-10)	IWI	10.4	756	105	0.506	0.045	50	0.9
Ti-SBA-16(I-20)	IWI	20.4	677	93	0.469	0.040	50	0.9
Ti-SBA-16(I-30)	IWI	29.7	596	76	0.429	0.033	49	0.9

[a] CG, chemical grafting; IWI, incipient wetness impregnation.
[b] Determined by chemical analysis.
[c] S_μ, micropore area; V_μ, micropore volume.
[d] Pore diameter determined from the adsorption isotherms by the BJH method.
[e] Normalized surface area calculated as $NS_{BET} = S_{BET,\ Ti\text{-}SBA\text{-}16}/S_{BET,\ Si\text{-}SBA\text{-}16}\ (1 - y)$ where y is the weight fraction of TiO_2 in the Ti-SBA-16 support.

The purely siliceous parent SBA-16 was prepared according to the previously described procedure [27,31], using a stirring time of 20 h at 25 °C, followed by an aging period of 24 h at 100 °C. The XRD pattern of this calcined sample (Fig. 1a) shows a very strong sharp (1 1 0) reflection (0.8° 2Θ) of the cubic $Im\bar{3}m$ structure and a small shoulder of the (2 0 0) reflection (1.15° 2Θ). These reflections yield an a_o value of 156 Å, confirming that the measured structure is indeed the $Im\bar{3}m$ structure [27]. Similar XRD pattern was also observed for the Ti-SBA-16(G-15) sample (Fig. 1b). When titanium isopropoxide is impregnated on the SBA-16 surface, the most intense (1 1 0) reflection can also be observed. However, its intensity decreases (Fig. 1c–e) indicating some loss in the long-range periodicity order of the SBA-16 sample. In all cases, the position of (1 1 0) reflection was the same as in the parent purely siliceous SBA-16, giving a_o a value of 156 Å.

Nitrogen adsorption–desorption isotherms of the parent Si-SBA-16 and Ti-containing SBA-16 samples are shown in Fig. 2. The very typical adsorption–desorption hysteresis, characteristic for ink-bottle pores of SBA-16 material, is clearly observed for both samples. The pore size distributions calculated from the adsorption branch of the isotherms show a narrow distribution of mesopores, distributed around an average pore diameter of 52 Å for Si-SBA-16 sample and around 50 Å for Ti-modified SBA-16 supports. For these materials, pore wall thickness (h_w) can be calculated from a simple formula $\delta = \sqrt{3}a_o/2 - D_P$ where D_P and a_o are the mesopore diameter and cubic unit cell parameter, respectively [38]. Pore wall thickness for the parent Si-SBA-16 sample was found to be equal to 83 Å. This value shows that the walls of Si-SBA-16 are about five times thicker than of the MCM-41-type materials. Titanium incorporation in the SBA-16 by post-synthetic methods does not produce changes in a_o value (Fig. 1). However, some decrease in pore diameter after Ti deposition (Table 1) makes evident a slight increase (2–3 Å) in pore wall thickness in Ti-containing samples, indicating that the titania species are deposited inside the mesopore channels of SBA-16. It is interesting to note that the increase in pore wall thickness is similar for all the Ti-containing samples prepared by chemical grafting and incipient wetness impregnation, and with different Ti loadings.

Nitrogen adsorption–desorption isotherms from the Ti-containing SBA-16 materials (Fig. 2b–e) keep the characteristic shape of the isotherm of the Si-SBA-16, indicating that post-synthetic incorporation of titanium by both methods

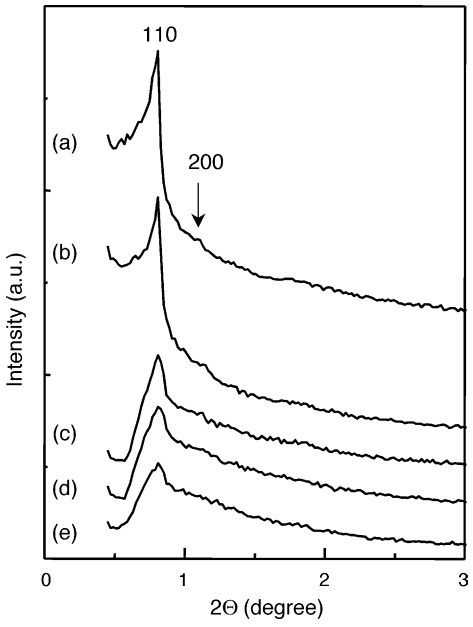

Fig. 1. Small-angle XRD patterns of Si-SBA-16 (a); Ti-SBA-16(G-15) (b); Ti-SBA-16(I-10) (c); Ti-SBA-16(I-20) (d) and Ti-SBA-16(I-30) (e) supports.

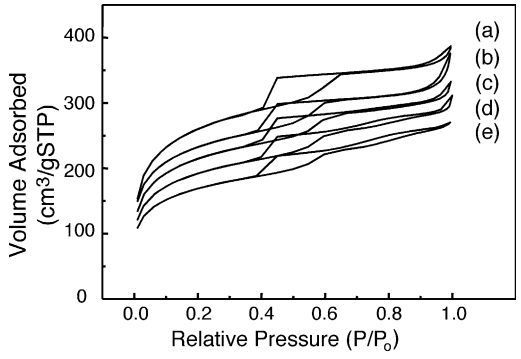

Fig. 2. Nitrogen adsorption–desorption isotherms of SBA-16 type supports: Si-SBA-16 (a); Ti-SBA-16(G-15) (b); Ti-SBA-16(I-10) (c); Ti-SBA-16(I-20) (d) and Ti-SBA-16(I-30) (e).

used does not affect the original pore structure of the parent material. However, the use of incipient wetness impregnation results in an appearance of a secondary porosity which is evidenced by new adsorption–desorption hysteresis at high relative pressure (P/P_o between 0.6 and 0.9) (Fig. 2d and e). The results of textural characterization (Table 1) show that the parent Si-SBA-16 possesses the highest surface area and pore volume. The post-synthetic Ti incorporation produces a significant decrease in the amount of the adsorbed N_2, reflecting drop in surface area and total pore volume. This decrease suggests the possibility of some pore blocking in the Ti-SBA-16 samples. However, if the measured surface areas of Ti-containing supports are corrected taking into account the weight of TiO_2 incorporated in the samples, and normalized surface areas are calculated as described in [15], it can be clearly observed that there is no pore blocking in Ti-SBA-16(G-15) support (Table 1) and only slight pore blocking takes place in Ti-SBA-16(I-*x*) series samples.

In line with previously reported results [30,31], all SBA-16 materials synthesised in the present work, purely siliceous and Ti-containing, have the combined micro- and mesoporosity (Table 1). In the starting Si-SBA-16 material, micropores represent about 12% of the total surface area (t-plot). It should be mentioned that the proportion of micropores in SBA-16-type materials can be significantly higher (up to 50%) depending on the conditions of the synthesis used [31]. The preparation procedure used in the present work was modified to reduce the microporosity, this was achieved by increasing the temperature of the hydrothermal treatment at aging stage from 80 °C (standard SBA-16 preparation procedure [27]) to 100 °C. The micro/mesopore structure is still maintained in the Ti-modified samples. It can be observed that Ti deposition does not produce significant blocking of micropores. Indeed, the proportion of micropores in Ti-SBA-16 samples is almost the same as in the parent Si-SBA-16.

Fig. 3 shows powder X-ray diffraction patterns of the supports. The diffractograms of the starting Si-SBA-16 and Ti-SBA-16(G-15) samples do not show the presence of any crystalline phase. In contrast, for Ti-SBA-16(I-*x*) samples the appearance of peaks in the 2Θ region between 3 and 90° due to crystalline TiO_2 was detected. In the diffractograms of the Ti-SBA-16(I-*x*) samples with 10.4 and 20.4 wt.% TiO_2, only two peaks indexed to the (1 0 1) and (2 0 0) reflections of anatase (JCPDS card 21–1272) were observed, whereas in the XRD pattern of the sample with higher TiO_2 loading (29.7%) most of the characteristic reflections of TiO_2-anatase were present. In line with this, the estimated size of the TiO_2 crystallites calculated by the Scherrer equation [39] increases from 278 to 373 Å with increase in TiO_2 loading from 10.4 to 29.7 wt.% TiO_2. The integral intensity of TiO_2-anatase (2 0 0) reflection (48.1° 2Θ) compared with calibration data was used to estimate the content of the TiO_2-anatase phase in Ti-SBA-16(I-*x*) supports. It was found that the amount of crystalline anatase phase changes from 2 to 9 wt.% TiO_2 with increase in titania loading from 10.4 to 29.7 wt.%. These results suggest that in the samples prepared by impregnation, only a minor fraction of titania is present on the external surface of the SBA-16 particles as anatase crystallites.

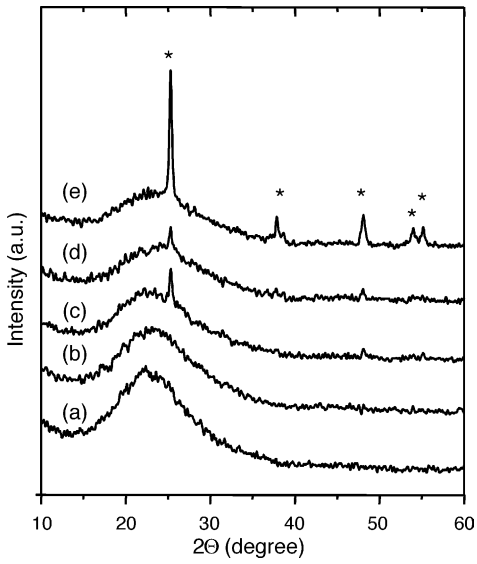

Fig. 3. Powder X-ray diffraction patterns of SBA-16 supports: Si-SBA-16 (a); Ti-SBA-16(G-15) (b); Ti-SBA-16(I-10) (c); Ti-SBA-16(I-20) (d) and Ti-SBA-16(I-30) (e). *TiO_2 anatase.

In line with the above results, in the Raman spectra of Ti-SBA-16 materials prepared by incipient wetness impregnation method (Fig. 4c–e), the characteristic bands of TiO_2-anatase [34,40] gradually appear at 147, 398, 517 and 640 cm^{-1} with increase in TiO_2 loading. This confirms that TiO_2 deposited on Si-SBA-16 by impregnation of a

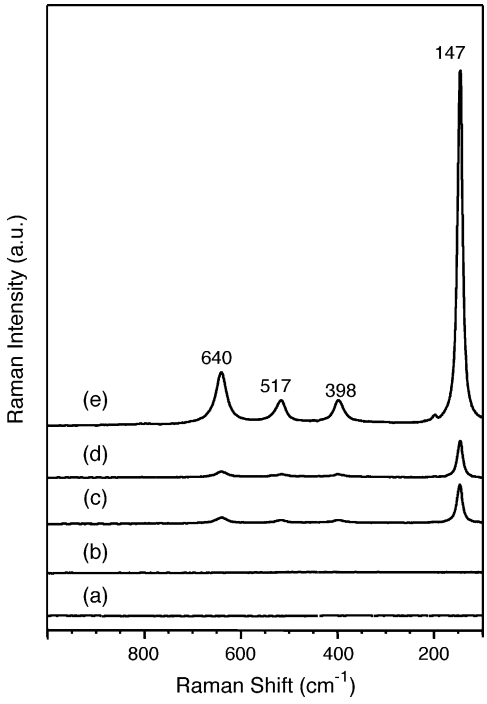

Fig. 4. FT–Raman spectra of Si-SBA-16 (a); Ti-SBA-16(G-15) (b); Ti-SBA-16(I-10) (c); Ti-SBA-16(I-20) (d) and Ti-SBA-16(I-30) (e) supports.

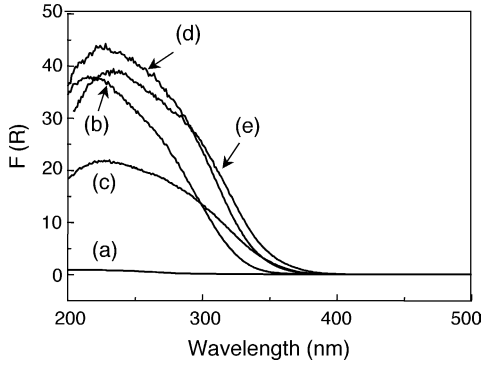

Fig. 5. UV–vis spectra of Si-SBA-16 (a); Ti-SBA-16(G-15) (b); Ti-SBA-16(I-10) (c); Ti-SBA-16(I-20) (d) and Ti-SBA-16(I-30) (e) supports.

$Ti(i\text{-}PrO)_4$ solution, exists as an anatase phase, even in the samples with low TiO_2 loading. The Raman spectrum of Ti-SBA-16(G-15) support prepared by chemical grafting (Fig. 4b) does not show any signal of titania anatase phase, confirming a good dispersion of titania species in this case.

Additional information about TiO_2 dispersion in the series of Ti-SBA-16 materials was obtained by UV–vis diffuse reflectance spectroscopy (Fig. 5). According to literature data, the DRS spectrum of bulk TiO_2-anatase exhibits a broad absorption at ~330 nm with an absorption edge at about 390 nm due to ligand-to-metal charge transfer between the O^{2-} ligand and the titanium(IV) ion [35]. No absorptions arise from silica, which is transparent in this region of the UV–vis spectrum (Fig. 5a). In the DRS spectrum of Ti-SBA-16(G-15) sample, the absorption band maximum is observed at 225 nm (Fig. 5b). The band at ca. 230 nm has been observed for various zeolite materials and has been assigned to ligand-to-metal charge transfer involving isolated Ti atoms in tetrahedral (T_d) coordination [35,41]. The shoulder at ca. 270 nm observed in the DRS spectrum of Ti-SBA-16(G-15) sample indicates the presence of some isolated or partially polymerized (Ti-O-Ti clusters) octahedral (O_h) titanium species [35,41,42]. The absence of an absorption at ~330 nm indicates that the sample prepared by the grafting method is free from anatase phase. These data altogether allow one to conclude that Ti is highly dispersed in Ti-SBA-16(G-15) sample. The Ti-SBA-16(I-*x*) samples prepared by impregnation are more susceptible to anatase formation and show clear absorption in the 300–330 nm region (Fig. 5c–e). The absorption band near 290 nm has been observed for dispersed TiO_2 nanoparticles on silica [43,44]. Red shift of the absorption edge is observed for Ti-SBA-16(I-*x*) samples with the increase in Ti loading suggesting an increase in the size of the Ti–O–Ti domains [43–45]. This result is consistent with the formation of TiO_2-anatase particles and their growth, which was observed by XRD and Raman spectroscopy. Additionally, the 230 nm band still present in the spectra of Ti-SBA-16(I-*x*) samples prepared by the impregnation method suggests that TiO_2 nanoparticles co-exist with the isolated Ti species in these supports. The detailed analysis of the spectra (c–e) in Fig. 5 shows that an increase in Ti loading in the samples produces not only an increase in the intensity of the UV–vis DRS spectra, but also changes the ratio between isolated tetrahedral Ti species and TiO_2 particles, increasing the proportion and the size of the latter.

From the results of characterization presented above, it is possible to conclude that the two methods of post-synthetic Ti incorporation tested in this study allowed preparation of a mesoporous SBA-16 type materials with relatively high TiO_2 loadings and without considerable decomposition of the initial SBA-16 structure. Chemical grafting of titanium species leads to Ti-SBA-16 supports with highly dispersed Ti species, but titanium loading in this case is limited by the number of reactive OH groups on the surface of the parent Si-SBA-16. The appearance of anatase signals in the XRD patterns, DRS and Raman spectra of samples prepared by the incipient wetness impregnation shows worse dispersion of TiO_2 in comparison with the sample prepared by chemical grafting. In addition, it was found that in the samples prepared by impregnation different Ti species are present simultaneously: isolated Ti species and small anatase clusters (inside the mesopore channels of SBA-16) and anatase crystallites (on the external surface). The relative proportion of different types of Ti species is easily changed with Ti loading. However, the titania loading that could be achieved with impregnation method is not limited as in chemical grafting.

3.2. Catalysts

Chemical analysis results show that the actual chemical composition (Ni and Mo loading) of all the prepared NiMo catalysts is close to the expected nominal one, 12 wt.% MoO_3 and 3 wt.% NiO (Table 2). The textural characteristics

Table 2
Actual compositions and textural characteristics of NiMo catalysts supported on SBA-16 type supports

Sample	Chemical composition[a] (wt.%)				S_{BET} (m^2/g)	S_μ[b] (m^2/g)	V_P (cm^3/g)	V_μ[b] (cm^3/g)	D_P[c] (Å)
	NiO	MoO_3	SiO_2	TiO_2					
NiMo/Si-SBA-16	2.9	12.1	85.0	0.0	555	66	0.413	0.030	50
NiMo/Ti-SBA-16(G-15)	3.0	12.1	72.1	12.8	493	61	0.378	0.029	45
NiMo/Ti-SBA-16(I-10)	3.1	12.0	75.7	9.2	470	52	0.361	0.023	46
NiMo/Ti-SBA-16(I-20)	3.1	11.9	67.3	17.7	412	48	0.314	0.021	46
NiMo/Ti-SBA-16(I-30)	2.9	12.2	59.5	25.4	336	33	0.271	0.014	46

[a] Determined by chemical analysis.
[b] S_μ, micropore area; V_μ, micropore volume.
[c] Pore diameter determined from the adsorption isotherms by the BJH method.

of NiMo catalysts supported on SBA-16 molecular sieves are given in Table 2. A significant decrease in surface area and pore volume is observed when Ni and Mo are incorporated to the support. For all NiMo/SBA-16 catalysts the decrease in support surface area is much stronger (38–44%) that can be explained taking into account the weight of deposited Ni and Mo species. This decrease is more pronounced for the catalysts supported on Ti-SBA-16(I-30), i.e., the support with the highest titania loading and subsequently lowest surface area and pore volume.

No changes were detected in the form of N_2 adsorption–desorption isotherms (not shown) after successive incorporation of Mo and Ni species to the SBA-16 support. A significant decrease in the amount of the adsorbed N_2 is observed after metal impregnation, especially after Mo deposition. However, the hysteresis loop maintains its shape characteristic of SBA-16 materials. In line with this, a characteristic (1 1 0) reflection of $Im\bar{3}m$ structure is still observed in the XRD pattern of all NiMo/SBA-16 catalysts, but a significant decrease in its intensity and broadening after Ni and Mo deposition suggests some loss in the periodicity of the SBA-16 pore structure. Therefore, a strong obstruction of the support pores or a partial collapse of its structure after metal deposition could be supposed to occur in these catalysts.

The incorporation of Ti atoms in the SBA-16 support by post-synthetic chemical grafting or impregnation improves only slightly the catalyst textural characteristics (Table 2). Additionally, a small reduction of pore size (from 50 to 46 Å) is observed in NiMo catalysts supported on all Ti-containing SBA-16 materials, which suggests that the deposited Mo and Ni oxide species are located inside the pores of Ti-modified SBA-16 supports.

Powder XRD patterns for NiMo catalysts supported on different SBA-16 materials show only the diffraction lines corresponding to reflections of TiO_2-anatase phase. Ni and Mo impregnation does not induce the detection of new XRD reflections, showing a good dispersion of Ni and Mo oxidic species in all catalysts. This result can be attributed to high surface area of all SBA-16 supports used in this study, as well as to the promotion effect of Ni addition. Therefore, XRD characterization was not able to reveal changes in the characteristics of Ni and Mo oxidic species induced by titanium addition to the SBA-16 support.

However, the TPR characterization of NiMo/SBA-16 catalysts (Fig. 6) shows clear differences in the characteristics of Ni and Mo oxidic species on pure siliceous and Ti-containing supports. The TPR profile of the NiMo/Si-SBA-16 sample exhibits three main reduction peaks at 392, 476 and 689 °C. The low temperature peak (392 °C) is associated generally with the first step of reduction from Mo^{6+} to Mo^{4+} of polymeric octahedral Mo species weakly bound to the silica surface (probably, small clusters of MoO_3 not detected by XRD) [46,47]. The second reduction peak may be assigned to the reduction of a $NiMoO_4$-like phase (the main peak at 475 °C) [48] or octahedral Mo species with higher degree of

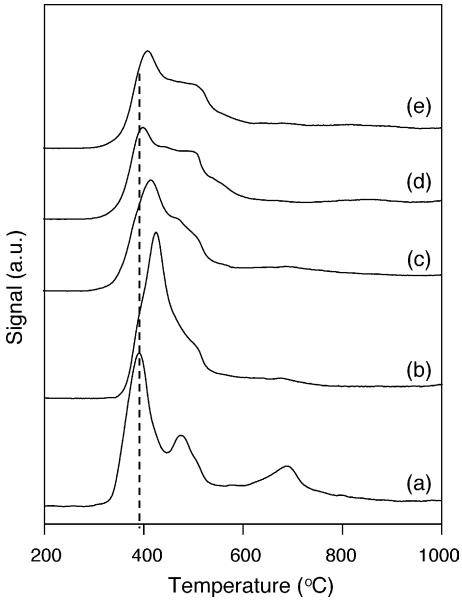

Fig. 6. TPR profiles for NiMo catalysts supported on Si-SBA-16 (a); Ti-SBA-16(G-15) (b); Ti-SBA-16(I-10) (c); Ti-SBA-16(I-20) (d) and Ti-SBA-16(I-30) (e).

polymerization. Finally, the peak at about 690 °C in the case of SiO_2-supported Mo catalysts is attributed to the second step of reduction of the MoO_3 species, from Mo^{4+} to Mo^0 [48]. The TPR characterization of NiMo catalysts supported on Ti-containing SBA-16 (Fig. 6) shows that Ti incorporation into the SBA-16 leads to an increase in the temperature of Ni and Mo reduction because of their stronger interaction with the Ti-containing support. Thus, the first step of reduction of polymeric octahedral Mo species in NiMo/Ti-SBA-16(G-15) sample takes place at 426 °C. The second reduction peak (at 475–480 °C) ascribed to the reduction of $NiMoO_4$-like species becomes less defined for all NiMo/Ti-SBA-16 catalysts. Additionally, Ti incorporation in SBA-16 results in appearance of a new reduction peak at about 500 °C, which is clearly observed in the TPR patterns of NiMo catalysts supported on Ti-SBA-16(I-20) and (I-30), Fig. 6d and e. The fact that this peak is well-defined when Ti-SBA-16 support has high TiO_2 loading and anatase crystals makes evident that this peak should be attributed to the reduction of Ni or Mo oxidic species in interaction with TiO_2-anatase phase. Previously it has been reported that the reduction of octahedrally coordinated Ni^{2+} ions in the Ni/TiO_2 samples ($NiTiO_3$-like structure) occurs at about 500 °C [48] indicating that in our catalysts these Ni species can also be present. Additional information can be obtained from the analysis of the shape of the obtained TPR patterns. It can be observed that the catalysts supported on Si-SBA-16 and Ti-SBA-16(G-15) show intense and sharp reduction peaks indicating homogeneity of the Ni and Mo surface species on the surface of these supports. However, when Ti-SBA-16(I-*x*) supports are prepared by impregnation, TPR patterns of NiMo catalysts are less defined. In low temperature region (300–600 °C), at least three reduction peaks can be observed reflecting the presence

of different types of Ni and Mo oxidic species in these samples. In line with this, at high temperatures (600–1000 °C) different peaks of the second step of the reduction of Mo^{4+} to Mo^0 are overlapped with titanium reduction in 600–800 °C region. All this shows the heterogeneity of the NiMo catalysts on Si-SBA-16(I-*x*) supports, which is probably induced by the heterogeneity of the support surface on which different Ti species, viz., highly dispersed ones, small anatase clusters, and large TiO_2 crystals, coexist.

HRTEM observations of the sulfided catalysts reflect the changes in the morphology of MoS_2 with titanium incorporation in the support. The typical fringes due to MoS_2 crystallites with 6.2 Å interplanar distances were observed on micrographs of all sulfided catalysts (Fig. 7). Previously it was shown, that in the Si-SBA-16 supported catalyst, MoS_2 crystallites with lengths between 20 and 60 Å and stacking from two to four layers are formed [32]. Ti incorporation in the SBA-16 material leads, in general, to better dispersion of MoS_2 active phase. Average length and layer number of the MoS_2 crystallites are present in Table 3. For all Ti-containing supports, a decrease was observed in the stacking degree of MoS_2 particles. The proportion of highly dispersed MoS_2 crystals formed by a single slab increased from 6% for NiMo/Si-SBA-16 catalyst to 11% for NiMo catalysts supported on Ti-SBA-16(G-15), and 12–18% for NiMo/Ti-SBA-16(I-*x*) samples (Fig. 8). In addition, a decrease in lengths of the MoS_2 structures was observed for NiMo/SBA-16 catalysts with Ti incorporation. The highest population of short MoS_2 crystals with the length <40 Å was found in NiMo/Ti-SBA-16(G-15) sample. A more detailed analysis of the slab length distribution in NiMo catalysts of a Ti-SBA-16(I-x) series (Fig. 8c–e) reveals that in this case the catalyst supported on Ti-SBA-16 with intermediate TiO_2 loading (20.4 wt.%) shows the lowest proportion of large MoS_2 crystals with the length >60 Å. Further increase in titania loading leads to an increment in the proportion of both, short (length <20 Å) and large (length >60 Å), MoS_2 crystals (Figs. 7 and 8). This result can be

Table 3
Average length and layer number of the MoS_2 crystallites

Sample	Average length (Å)	Average stacking
NiMo/Si-SBA-16	39.5	3.4
NiMo/Ti-SBA-16(G-15)	35.4	3.0
NiMo/Ti-SBA-16(I-10)	42.0	3.1
NiMo/Ti-SBA-16(I-20)	37.7	2.8
NiMo/Ti-SBA-16(I-30)	37.6	2.9

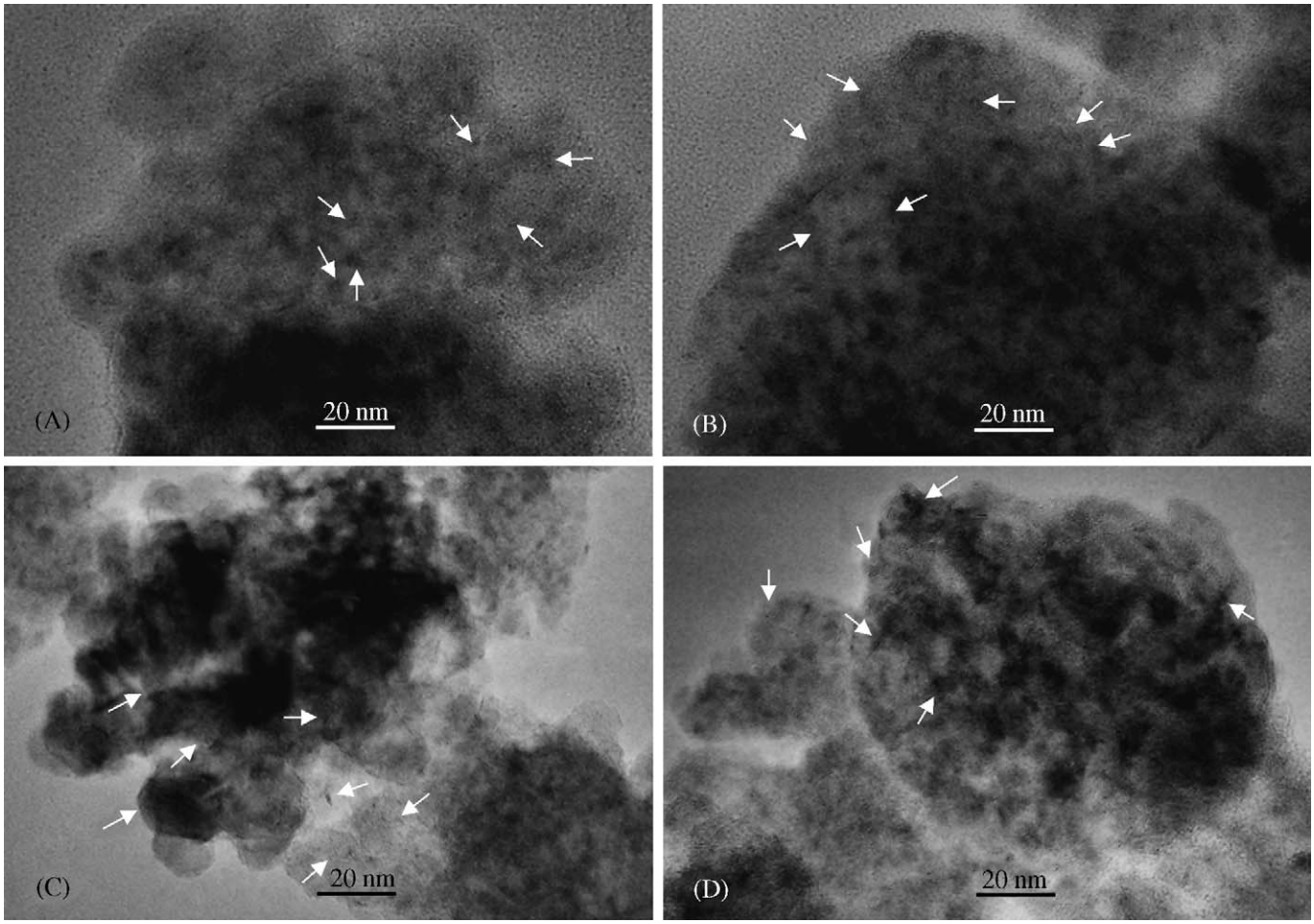

Fig. 7. HRTEM micrographs for sulfided NiMo catalysts supported on Ti-SBA-16(G-15) (A); Ti-SBA-16(I-10) (B); Ti-SBA-16(I-20) (C) and Ti-SBA-16(I-30) (D).

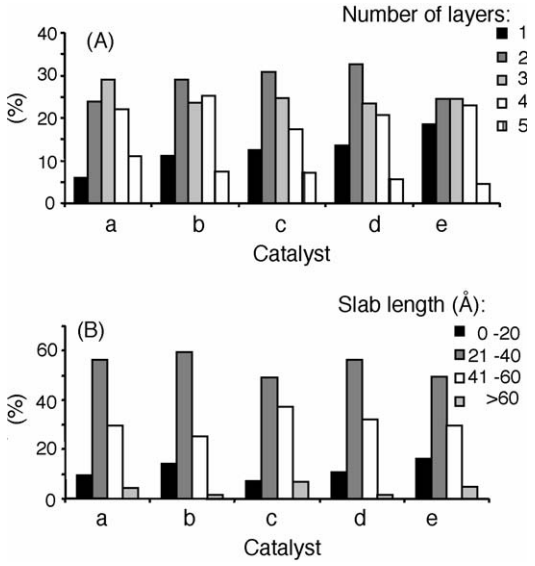

Fig. 8. Layer stacking (A) and length (B) distribution of MoS_2 crystallites in sulfided NiMo catalysts supported on Si-SBA-16 (a); Ti-SBA-16(G-15) (b); Ti-SBA-16(I-10) (c); Ti-SBA-16(I-20) (d) and Ti-SBA-16(I-30) (e).

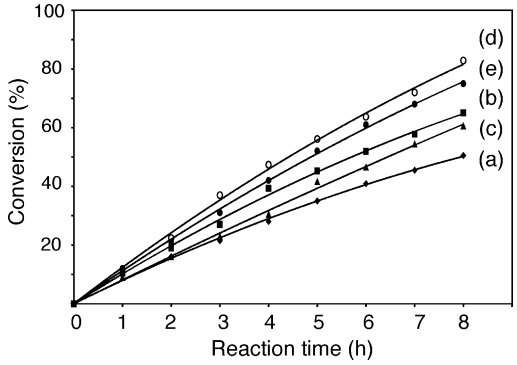

Fig. 9. 4,6-Dimethyldibenzothiophene (4,6-DMDBT) conversions obtained over NiMo catalysts supported on Si-SBA-16 (a); Ti-SBA-16(G-15) (b); Ti-SBA-16(I-10) (c); Ti-SBA-16(I-20) (d) and Ti-SBA-16(I-30) (e).

explained taking into consideration that high titania loading in the support may result in two opposite effects. On one side, the presence of TiO_2 anatase crystals provides good dispersion to Mo sulfided species supported on anatase surface. But on the other side, supports with low surface area and pore volume are obtained, and consequently, their dispersion capacity decreases.

3.3. Catalytic activity

In the present study, the catalytic activity of sulfided NiMo/SBA-16 catalysts was examined in the hydrodesulfurization of 4,6-dimethyldibenzothiophene, one of the most refractory sulfur compounds in gas oil [49]. The conversion of 4,6-DMDBT is shown in Table 4 and Fig. 9. It can be observed that 4,6-DMDBT conversion reached at 8 h changes in a wide range. Thus, the lowest 4,6-DMDBT conversion (50%) was observed for the catalyst supported on purely siliceous SBA-16. Catalytic activities of all NiMo catalysts supported on Ti-modified SBA-16 resulted to be significantly higher reaching the maximum conversion of 83% with NiMo/Ti-SBA-16(I-20) catalyst. However, further increase in the titania loading in the support up to 29.7 wt.% TiO_2 leads to some decrease in the catalytic activity. Previously similar activity trend was observed for NiMo catalysts supported on TiO_2–Al_2O_3 mixed oxides in thiophene HDS, where the maximum catalytic activity was found in the support with 17 wt.% TiO_2 [48]. This maximum in catalytic activity was attributed to the "formation of an active phase with an optimal composition of the oxidic precursors". In our case, the activity trend with the change in the Ti-containing SBA-16 support seems to be the result of two opposite effects. On one hand, the incorporation of titanium onto the support surface provides a stronger metal-support interaction, allowing better dispersion of the molybdenum and nickel oxidic and sulfided phases. This explains an increase in 4,6-DMDBT conversion with TiO_2 loading in NiMo/Ti-SBA-16 catalysts. On the other hand, this tendency is not linear, and when titania loading is too high, as in the case of NiMo/Ti-SBA-16(I-30) catalyst, a support with low surface area and porosity is obtained, in which the formation of large TiO_2 anatase crystals and some pore pluggings are observed. This leads to the catalysts in which not only the proportion of highly dispersed MoS_2

Table 4
4,6-DMDBT conversions and reaction product compositions obtained over NiMo/Ti-SBA-16 catalysts

Catalyst	4,6-DMDBT conversion[a] (%)	Product composition[b] (%)					HYD/DDS ratio[c]
		THDMDBT	HHDMDBT	MCHT	DMBP	DMBCH	
NiMo/Si-SBA-16	50	20.1	4.9	53.4	11.3	10.3	7.85
NiMo/Ti-SBA-16(G-15)	65	15.5	4.0	58.7	10.2	11.6	8.80
NiMo/Ti-SBA-16(I-10)	61	12.3	3.5	63.0	8.5	12.7	10.76
NiMo/Ti-SBA-16(I-20)	83	10.4	2.6	64.6	6.8	15.6	13.71
NiMo/Ti-SBA-16(I-30)	73	8.3	2.4	64.7	7.3	17.3	12.70

[a] At 8 h reaction time.

[b] Determined at 50% of total 4,6-DMDBT conversion. DDS, direct desulfurization pathway; HYD, hydrogenation pathway; THDMDBT, tetrahydrodimethyldibenzothiophene; HHDMDBT, hexahydrodimethyldibenzothiophene; MCHT, methylcyclohexyltoluene; DMBP, dimethylbiphenyl; DMBCH, dimethylbicyclohexyl.

[c] HYD/DDS pathway ratio was determined as the ratio of HYD route products (THDMDBT + HHDMDBT + MCHT + DMBCH) to DDS route product (DMBP) [51].

species, but also that of the agglomerated ones increases. As a result, the total catalytic activity slightly decreases.

Nowadays, it is known that the HDS of methyl-substituted DBT derivatives occurs through two parallel reactions, namely (i) direct desulfurization (DDS) yielding the corresponding substituted biphenyl (BP) products and (ii) hydrogenation with subsequent desulfurization (HYD), yielding first substituted tetrahydrodibenzothiophenes, then the corresponding hexahydro derivatives and, finally cyclohexylbenzene-type compounds [20,50,51]. Previously, it has been shown that under HDS conditions (i.e., in presence of an organic sulfur compound) biphenyl-type compounds do not hydrogenate readily into cyclohexylbenzene [51,52]. To elucidate the effect of Ti incorporation in the supports on the reaction pathways of 4,6-dimethyldibenzothiophene, the reaction product distributions at the same total 4,6-DMDBT conversion (50%) was compared for different catalysts (Table 4). The detailed analysis of the reaction products shows that for all catalysts studied the preferential pathway is HYD. When Ti-atoms are incorporated into the SBA-16 support, the proportion of HYD route products increases, reaching the maximum HYD/DDS ratio of 13.71 for the most active catalyst, NiMo/Ti-SBA-16(I-20). From Table 4 it can also be observed that an increase in the TiO_2 loading leads to a decrease in the proportion of tetrahydro- and hexahydrodibenzothiophene intermediates, and to an increase in the amount of desulfurized products of the HYD route, namely methylcyclohexyltoluene and dimethylbicyclohexyl. Therefore, titanium addition to the catalytic support enhances preferentially the desulfurization of previously hydrogenated intermediates.

4. Conclusions

According to the above results, the following conclusions can be stated.

Ti-containing SBA-16 type materials with relatively high Ti loadings and without considerable degradation of the initial SBA-16 structure can be prepared by post-synthetic methods (chemical grafting and incipient wetness impregnation). The characteristics of the Ti-SBA-16 supports change depending on the preparation method used and TiO_2 loading. Chemical grafting of Ti species leads to Ti-SBA-16 supports with highly dispersed Ti species, but titanium loading in this case is limited by the number of OH groups on the surface of parent Si-SBA-16. The appearance of anatase signals in the XRD patterns, DRS and Raman spectra of samples prepared by the incipient wetness impregnation method shows worse dispersion of TiO_2 in comparison with the sample prepared by chemical grafting. In addition, in the samples prepared by impregnation different Ti species are present simultaneously, viz., isolated Ti species and small anatase clusters (inside the mesopore channels of SBA-16) and large anatase crystals (on the external surface). The relative proportion of different types of Ti species is easily changed with TiO_2 loading.

The interaction of Ni and Mo species with the support becomes stronger with Ti loading into the SBA-16. According to this, the dispersion of sulfided Mo species increases.

NiMo catalysts supported on Ti-containing SBA-16 molecular sieves show high activity in HDS of refractory dibenzothiophenes (4,6-DMDBT). This activity increases with titania loading in the support reaching the maximum catalytic activity at 20.4 wt.% TiO_2 loading. Further increase in TiO_2 loading results in less active NiMo catalysts with low surface area and porosity. This points out the suitable methods of incorporation of titanium into the SBA type materials and optimum TiO_2 loadings for the preparation of active HDS catalysts.

Acknowledgements

Financial support by DGAPA-UNAM (grant IN-103102) is gratefully acknowledged. The authors wish to thank Manuel Aguilar-Franco for technical assistance with small-angle XRD characterizations.

References

[1] B.C. Gates, H. Topsøe, Polyhedron 16 (1997) 3213.
[2] F. van Looij, P. van der Laan, W.H.J. Stork, D.J. DiCamillo, J. Swain, Appl. Catal. A: General 170 (1998) 1.
[3] H. Shimada, T. Sato, Y. Yoshimura, J. Hiraishi, A. Nishijima, J. Catal. 110 (1988) 275.
[4] Y.I. Yermakov, A.N. Startsev, V.A. Burmistrov, Appl. Catal. 11 (1984) 1.
[5] M. Zdrazil, Catal. Today 86 (2003) 151.
[6] S.K. Maity, M.S. Rana, B.N. Srinivas, S.K. Bej, G. Murali Dhar, T.S.R. Prasad Rao, J. Mol. Catal. A 153 (2000) 127.
[7] H. Shimada, Catal. Today 86 (2003) 17.
[8] J.J. Lee, S. Han, H. Kim, J.H. Koh, T. Hyeon, S.H. Moon, Catal. Today 86 (2003) 141.
[9] Y. Okamoto, Catal. Today 39 (1997) 45.
[10] F. Bataille, J.L. Lemberton, G. Pérot, P. Leyrit, T. Cseri, N. Marchal, S. Kasztelan, Appl. Catal. A: General 220 (2001) 191.
[11] A. Wang, Y. Wang, T. Kabe, Y. Chen, A. Ishihara, W. Qian, J. Catal. 199 (2001) 19.
[12] T. Klimova, M. Calderón, J. Ramírez, Appl. Catal. A: General 240 (2003) 29.
[13] U.T. Turaga, C. Song, Catal. Today 86 (2003) 129.
[14] A. Wang, Y. Wang, T. Kabe, Y. Chen, A. Ishihara, W. Qian, P. Yao, J. Catal. 210 (2002) 319.
[15] L. Vradman, M.V. Landau, M. Herskowitz, V. Ezersky, M. Talianker, S. Nikitenko, Y. Koltypin, A. Gedanken, J. Catal. 213 (2003) 163.
[16] G. Murali Dhar, B.N. Srinivas, M.S. Rana, M. Kumar, S.K. Maity, Catal. Today 86 (2003) 45.
[17] T. Klimova, D. Solís, J. Ramírez, A. López-Agudo, Stud. Surf. Sci. Catal. 143 (2002) 267.
[18] J. Ramírez, R. Contreras, P. Castillo, T. Klimova, R. Zárate, R. Luna, Appl. Catal. A: General 197 (2000) 69.
[19] M. Breysse, P. Afanasiev, C. Geantet, M. Vrinat, Catal. Today 86 (2003) 5.
[20] S. Yoshinaka, K. Segawa, Catal. Today 45 (1998) 293.
[21] Z.B. Wei, W. Yan, H. Zhang, T. Ren, Q. Xin, Z. Li, Appl. Catal. A: General 167 (1998) 39.
[22] S. Dzwigaj, C. Louis, M. Breysse, M. Cattenot, V. Bellière, C. Geantet, M. Vrinat, P. Blanchard, E. Payen, S. Inoue, H. Kudo, Y. Yoshimura, Appl. Catal. B: Environ. 41 (2003) 181.

[23] T. Klimova, E. Rodríguez, M. Martínez, J. Ramírez, Micropor. Mesopor. Mater. 44–45 (2001) 357.
[24] P.J. Kooyman, P. Waller, A.D. van Langeveld, C. Song, K.M. Reddy, J.A.R. van Veen, Catal. Lett. 90 (2003) 131.
[25] Z. Li, L. Gao, S. Zheng, Appl. Catal. A: General 236 (2002) 163.
[26] D. Zhao, J. Feng, Q. Huo, N. Melosh, G.H. Fredrickson, B.F. Chmelka, G.D. Stucky, Science 279 (1998) 548.
[27] D. Zhao, Q. Huo, J. Feng, B.F. Chmelka, G.D. Stucky, J. Am. Chem. Soc. 120 (1998) 6024.
[28] T. Yamada, H. Zhou, K. Asai, I. Honma, Mater. Lett. 56 (2002) 93.
[29] Y. Bennandja, P. Beaunier, D. Margolese, A. Davidson, Micropor. Mesopor. Mater. 44–45 (2001) 147.
[30] C.-F. Cheng, Y.-C. Lin, H.-H. Cheng, Y.-C. Chen, Chem. Phys. Lett. 382 (2003) 496.
[31] P. Van Der Voort, M. Benjelloun, E.F. Vansant, J. Phys. Chem. B 106 (2002) 9027.
[32] T. Klimova, L. Lizama, J.C. Amezcua, P. Roquero, E. Terrés, J. Navarrete, J.M. Domínguez, Catal. Today 98 (2004) 141.
[33] Y. Sakamoto, M. Kaneda, O. Terasaki, D.Y. Zhao, J.M. Kim, G. Stucky, H.J. Shin, R. Ryoo, Nature 408 (2000) 449.
[34] M.S. Morey, S. O'Brien, S. Schwarz, G.D. Stucky, Chem. Mater. 12 (2000) 898.
[35] Z. Luan, E.M. Maes, P.A.W. van der Heide, D. Zhao, R.S. Czernuszewicz, L. Kevan, Chem. Mater. 11 (1999) 3680.
[36] I.G. Shenderovich, G. Buntkowsky, A. Schreiber, E. Gedat, S. Sharif, J. Albrecht, N.S. Golubev, G.H. Findenegg, H.-H. Limbach, J. Phys. Chem. B 107 (2003) 11924.
[37] S. Srinivasan, A.K. Datye, M.H. Smith, C.H.F. Peden, J. Catal. 145 (1994) 565.
[38] P.I. Ravikovitch, A.V. Neimark, Langmuir 18 (2002) 911.
[39] H.P. Klug, L.E. Alexander, X-Ray Diffraction Procedures for Polycrystalline and Amorphous Materials, John Wiley & Sons Inc., NY, 1954 , p. 530.
[40] U. Balachandran, N.G. Eror, J. Solid State Chem. 42 (1982) 276.
[41] S. Klien, B.M. Weckhuysen, J.A. Martens, W.F. Maier, P.A. Jacobs, J. Catal. 163 (1996) 489.
[42] G. Petrini, A. Cesana, G. De Alberti, F. Genoni, G. Leofanti, M. Padovan, G. Paparatto, P. Roffia, Stud. Surf. Sci. Catal. 68 (1991) 761.
[43] B.J. Aronson, C.F. Blanford, A. Stein, Chem. Mater. 9 (1997) 2842.
[44] Z. Luan, L. Kevan, Micropor. Mesopor. Mater. 44–45 (2001) 337.
[45] A. Fernandez, J. Leyrer, A.R. González-Elipe, G. Munuera, H. Knözinger, J. Catal. 112 (1988) 489.
[46] R. López Cordero, A. López Agudo, Appl. Catal. A: General 202 (2000) 23.
[47] R. López Cordero, F.J. Gil Llambias, A. López Agudo, Appl. Catal. 74 (1991) 125.
[48] S. Damyanova, A. Spojakina, K. Jiratova, Appl. Catal. A: General 125 (1995) 257.
[49] B.C. Gates, H. Topsøe, Polyhedron 16 (1997) 3213.
[50] C. Pophal, F. Kameda, K. Hoshino, S. Yoshinaka, K. Segawa, Catal. Today 39 (1997) 21.
[51] F. Bataille, J.L. Lemberton, P. Michaud, G. Pérot, M. Vrinat, M. Lemaire, E. Schulz, M. Breysse, S. Kasztelan, J. Catal. 191 (2000) 409.
[52] P. Michaud, J.L. Lemberton, G. Pérot, Appl. Catal. A: General 169 (1998) 343.